Supporting Information

for

Conformational properties of and a Reorientation Triggered by Sugar–Water Vibrational Resonance in the Hydroxymethyl Group in Hydrated β-Glucopyranose

Teppei Suzuki,* Hirotaka Kawashima, and Takayuki Sota

Integrative Bioscience and Biomedical Engineering, Graduate School of Science and Engineering, Waseda University, 3-4-1 Okubo, Shinjuku, Tokyo 169-8555, Japan

*Corresponding author. E-mail: teppei_suzuki@moegi.waseda.jp

This Supporting Information contains the following: hydroxymethyl rotamer populations for β-glucopyranose in D_2O using several sets of three values for the O5–C5–C6–O6 torsion angle, Table S1; dependence of the population of the *tg* (T) rotamer of β-glucopyranose in D_2O on the three O5–C5–C6–O6 torsion-angle values used for determining the limiting values for $^3J_{H5,H6,}$ Table S2; time series of the C6–O6 and O6–H6 distances during −0.5–0.7 ps, Figure S2; time series of the O6–C6–O_{D1} and O6–C6–O_{D2} angles, Figure S3; time-frequency spectrum for the C6–O6–H6 bending mode in the simulation (i) and the corresponding instantaneous amplitudes, Figure S4; time evolution of the estimated vibrational energies for the C6–O6 and O6–H6 stretching vibrations in the simulation (i) for the entire region, Figure S5; role of the low-frequency dynamics of the O6-H6 stretching motion in the prolonged strong O6-H6 stretching-mode vibrational energy during the pretransition period, Figure S6.

TABLE S1: Hydroxymethyl Rotamer Populations[a] (%) for β-Glucopyranose in D_2O Using Several Sets of Three Values for the O5–C5–C6–O6 Torsion Angle

the O5–C5–C6–O6 torsion angle (deg)			G^- (*gg*)	G^+ (*gt*)	T (*tg*)
(−60,	60,	180)[b]	43	56	1
(−65,	65,	180)	39	54	7
(−65,	65,	175)	38	55	7
(−70,	70,	175)	34	55	11
(−67,	65	175)[c]	38	54	8
(−64,	67,	153)[d]	31	59	10

[a] With the new equations proposed by Stenutz et al. [S1], we calculated the hydroxymethy rotamer populations for β-glucopyranose in D_2O, using the values for *J*-coupling constants previously reported by Nishida et al. [S2] ($^3J_{H5,\,H6R}$ and $^3J_{H5,\,H6S}$ are 6.0 and 2.1 Hz, respectively). [b] The perfectly staggered conformations. [c] Originally suggested values by Nishida et al. [S2]. [d] The average values obtained by our *ab initio* molecular dynamics simulations.

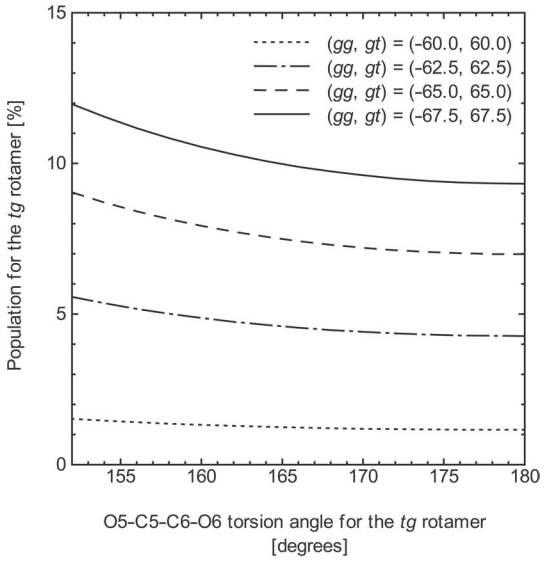

Figure S1. Dependence of the population of the *tg* (T) rotamer of β-glucopyranose in D_2O on the three O5–C5–C6–O6 torsion-angle values used for determining the limiting values for $^3J_{H5,H6}$. With the new equations proposed by Stenutz et al. [S1], we calculated the T rotamer populations for β-glucopyranose in D_2O, using the values for *J*-coupling constants previously reported by Nishida et al. [S2] ($^3J_{H5,\,H6R}$ and $^3J_{H5,\,H6S}$ are 6.0 and 2.1 Hz, respectively).

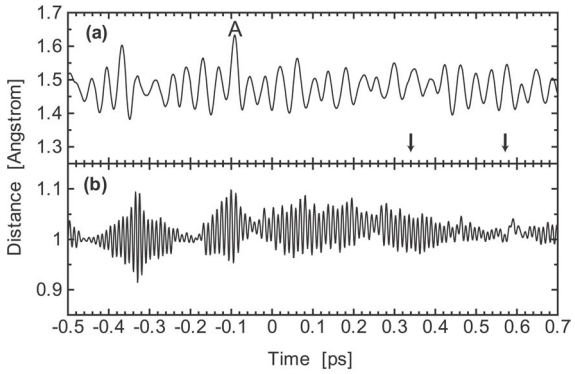

Figure S2. Time series of the C6–O6 (a) and O6–H6 distances during −0.5–0.7 ps. The time origin is the starting point of the NVE simulation. The arrows in (a) are the starting and final points of the transitions (about 0.34 and 0.57 ps, respectively). Label A indicates the point where the amplitudes of the C6–O6 and O6–H distances were relatively large. Note that in the NVT simulation (−0.5–0.0 ps) the dynamics was substantially restricted by the Nosé–Hoover chain thermostat method (ref S3).

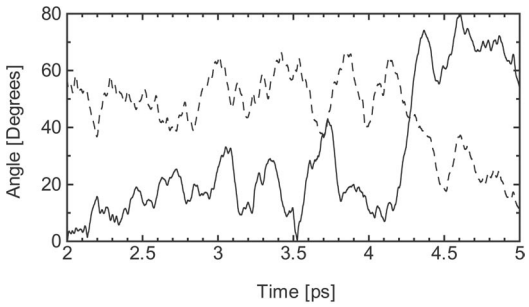

Figure S3. Time series of the O6–C6–O_{D1} (solid line) and O6–C6–O_{D2} (dashed line) angles. For the definition of O_{D1} and O_{D2}, see Figure 3a.

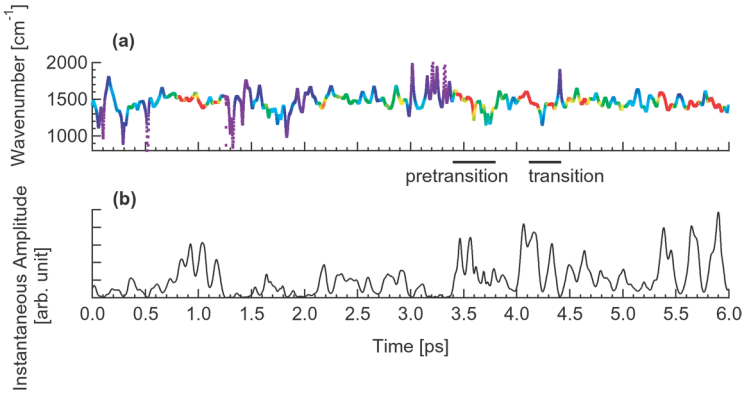

Figure S4. Time-frequency spectrum for the C6–O6–H6 bending mode in the simulation (i) (part a) and the corresponding instantaneous amplitudes (part b). The frequency region in part a corresponds to the first band at the fourth level. The time-frequency spectrum was obtained using the maximal-overlap discrete wavelet packet transform and the Hilbert transform (the convolution theorem was used). A scaling factor of 1.1 was used.

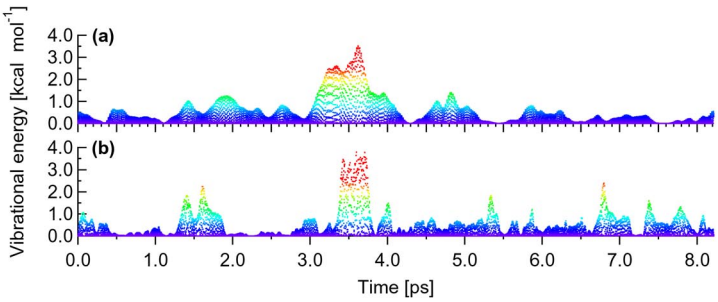

Figure S5. Time evolution of the estimated vibrational energies for the C6–O6 (a) and O6–H6 (b) stretching vibrations in the simulation (i) for the entire region. For our estimates, see the text.

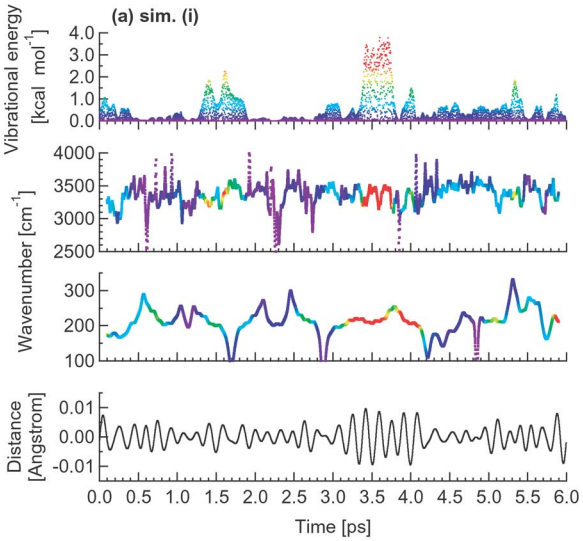
(a) sim. (i)
Vibrational energy [kcal mol^{-1}]
Wavenumber [cm^{-1}]
Distance [Angstrom]
Time [ps]

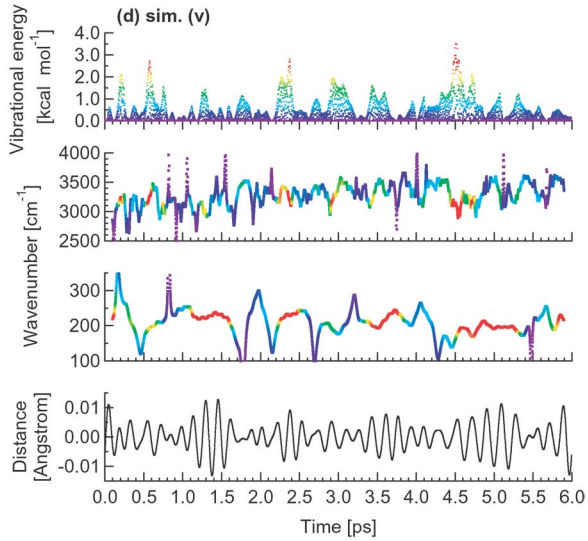
(d) sim. (v)
Vibrational energy [kcal mol^{-1}]
Wavenumber [cm^{-1}]
Distance [Angstrom]
Time [ps]

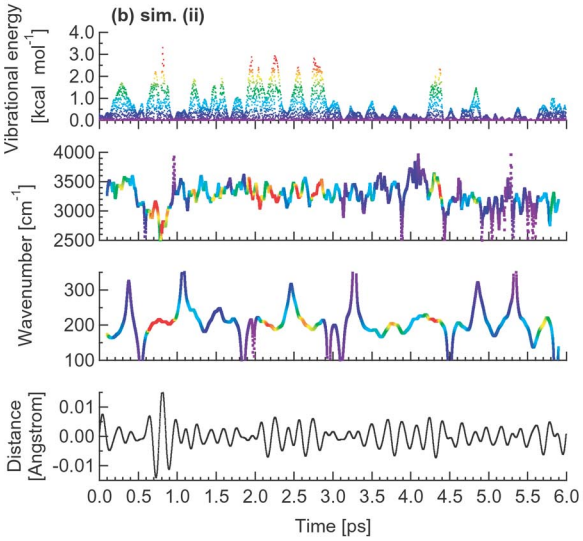
(b) sim. (ii)
Vibrational energy [kcal mol^{-1}]
Wavenumber [cm^{-1}]
Distance [Angstrom]
Time [ps]

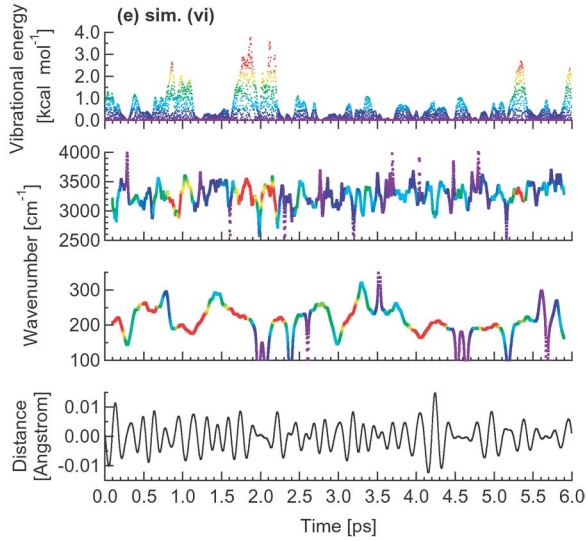
(e) sim. (vi)
Vibrational energy [kcal mol^{-1}]
Wavenumber [cm^{-1}]
Distance [Angstrom]
Time [ps]

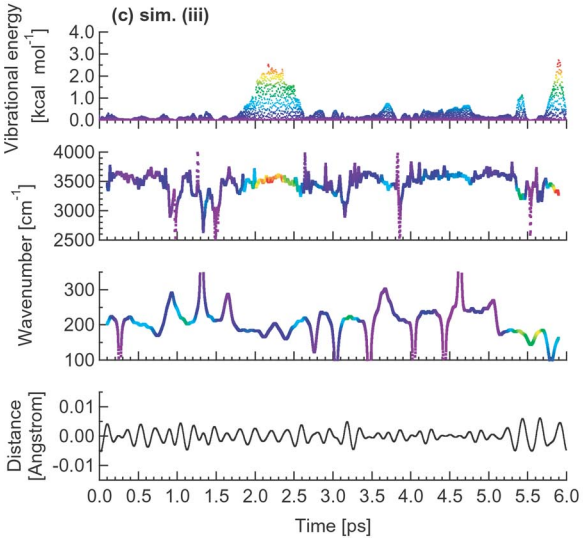
(c) sim. (iii)
Vibrational energy [kcal mol^{-1}]
Wavenumber [cm^{-1}]
Distance [Angstrom]
Time [ps]

Figure S6. Role of the low-frequency dynamics of the O6-H6 stretching motion during the prolonged strong O6-H6 stretching-mode vibrational energy during the pretransition period. The low-frequency dynamics of the O6–H6 stretching motion in the trajectory that underwent the reorientation [part a, the simulation (i)] is compared with the ones in the trajectories that did not underwent a rotational transition [part b, the simulation (ii); part c, the simulation (iii); part d, the simulation (v); part e, the simulation (vi)]. Each part is composed of four panels (from top to bottom): the O6-H6 stretching-mode vibrational energy; the O6–H6 stretching-mode frequency in the 2500–4000 cm^{-1} (the first band at the third level); the low-frequency region for the O6–H6 stretching motion (100–350 cm^{-1}) (the first band at the seventh level); the decomposed component motion in the 100–350 cm^{-1}. The time-frequency spectra were obtained using the maximal-overlap discrete wavelet packet transform and the Hilbert transform (for the first band at the third level, the convolution theorem was used, whereas, for the first band at the seventh level, the normal definition for the Hilbert transform was used). No cutoff for instantaneous amplitudes was used. Part a shows that, during the prolonged strong O6–H6 stretching-mode vibrational energy (the pretransition region), the low-frequency dynamics was also involved (see 3.3–4.0 ps).

References for Supporting Information

[S1] Stenutz, R.; Carmichael, I.; Widmalm, G.; Serianni, A. S. *J. Org. Chem.* **2002**, *67*, 949.

[S2] (a) Nishida, Y.; Ohrui, H.; Meguro, H. *Tetrahedron Lett.* **1984**, *25*, 1575. (b) Nishida, Y.; Hori, H.; Ohrui, H.; Meguro, H. *J. Carbohydr. Chem.* **1988**, *7*, 239.

[S3] Tuckerman, M. E.; Parrinello, M. *J. Chem. Phys.* **1994**, *101*, 1302.